



University
of Glasgow

Phillips, D.B., Simpson, S.H., Grieve, J.A., Gibson, G.M., Bowman, R. ,
Padgett, M. , Miles, M.J., and Carberry, D.M. (2011) *Position clamping
of optically trapped microscopic non-spherical probes*. Optics Express,
19 (21). pp. 20622-20627. ISSN 1094-4087 (doi:10.1364/OE.19.020622)

<http://eprints.gla.ac.uk/59793/>

Deposited on: 11th September 2012

Position clamping of optically trapped microscopic non-spherical probes

D. B. Phillips,¹ S. H. Simpson,¹ J. A. Grieve,¹ G. M. Gibson,²
R. Bowman,² M. J. Padgett,² M. J. Miles,¹ and D. M. Carberry^{1,*}

¹ *H. H. Wills Physics Laboratories, University of Bristol, Bristol, England, United Kingdom*

² *SUPA, Department of Physics and Astronomy, University of Glasgow, Glasgow, Scotland, United Kingdom*

**david.carberry@bristol.ac.uk*

Abstract: We investigate the degree of control that can be exercised over an optically trapped microscopic non-spherical force probe. By position clamping translational and rotational modes in different ways, we are able to dramatically improve the position resolution of our probe with no reduction in sensitivity. We also demonstrate control over rotational-translational coupling, and exhibit a mechanism whereby the average centre of rotation of the probe can be displaced away from its centre.

© 2011 Optical Society of America

OCIS codes: (140.7010) Laser trapping; (170.4520) Optical confinement and manipulation.

References and links

1. A. Ashkin, J. Dziedzic, J. Bjorkholm, and S. Chu, "Observation of a single-beam gradient force optical trap for dielectric particles," *Opt. Lett.* **11**(5), 288–290 (1986).
2. D. Grier, "A revolution in optical manipulation," *Nature* **424**(6950), 810–816 (2003).
3. P. J. Rodrigo, V. R. Daria, and J. Glückstad, "Real-time three-dimensional optical micromanipulation of multiple particles and living cells," *Opt. Lett.* **29**(19), 2270–2272 (2004).
4. S. H. Simpson and S. Hanna, "Thermal motion of a holographically trapped SPM-like probe," *Nanotechnology* **20**(39), 395710 (2009).
5. O. M. Marago, P. H. Jones, F. Bonaccorso, V. Scardaci, P. G. Gucciardi, A. G. Rozhin, and A. C. Ferrari, "Femtonewton force sensing with optically trapped nanotubes," *Nano Lett.* **8**(10), 3211–3216 (2008).
6. F. C. Cheong and D. G. Grier, "Rotational and translational diffusion of copper oxide nanorods measured with holographic video microscopy," *Opt. Exp.* **18**(7), 6555–6562 (2010).
7. D. B. Phillips, D. M. Carberry, S. H. Simpson, H. Schaefer, M. Steinhart, R. Bowman, G. M. Gibson, M. J. Padgett, S. Hanna, and M. J. Miles, "Optimizing the optical trapping stiffness of holographically trapped microrods using high-speed video tracking," *J. Opt.* **13**(4, Sp. Iss. SI), 044023 (2011).
8. D. M. Carberry, S. H. Simpson, J. A. Grieve, Y. Wang, H. Schaefer, M. Steinhart, R. Bowman, G. M. Gibson, M. J. Padgett, S. Hanna, and M. J. Miles, "Calibration of optically trapped nanotools," *Nanotechnology* **21**(17) 175501 (2010).
9. T. Asavei, V. L. Y. Loke, M. Barbieri, T. A. Nieminen, N. R. Heckenberg, and H. Rubinsztein-Dunlop, "Optical angular momentum transfer to microrotors fabricated by two-photon photopolymerization," *New J. Phys.* **11**, 093021 (2009).
10. K. D. Wulff, D. G. Cole, and R. L. Clark, "Servo control of an optical trap," *Appl. Opt.* **46**(22), 4923–4931 (2007).
11. H. Ojala, A. Korsback, A. E. Wallin, and E. Haeggstrom, "Optical position clamping with predictive control," *Appl. Phys. Lett.* **95**(18), 181104 (2009).
12. Y. Huang, Z. Zhang, and C.-H. Menq, "Minimum-variance Brownian motion control of an optically trapped probe," *Appl. Opt.* **48**(30), 5871–5880 (2009).
13. D. Preece, R. Bowman, A. Linnenberger, G. Gibson, S. Serati, and M. Padgett, "Increasing trap stiffness with position clamping in holographic optical tweezers," *Opt. Express* **17**(25), 22718–22725 (2009).
14. G. Gibson, D. M. Carberry, G. Whyte, J. Leach, J. Courtial, J. C. Jackson, D. Robert, M. Miles, and M. Padgett, "Holographic assembly workstation for optical manipulation," *J. Opt.* **A10**(4), 044009 (2008).

15. D. B. Phillips, J. A. Grieve, S. N. Olof, S. J. Kocher, R. Bowman, M. J. Padgett, M. J. Miles, and D. M. Carberry, "Surface imaging using holographic optical tweezers," *Nanotechnology* **22**(28), 285503 (2011).
 16. R. Bowman, G. Gibson, and M. Padgett, "Particle tracking stereomicroscopy in optical tweezers: control of trap shape," *Opt. Express* **18**(11), 11,785–11,790 (2010).
-

1. Introduction

Optical tweezers use the high intensity gradients produced in a tightly focussed laser beam to trap micron sized dielectric particles [1]. For small displacements from equilibrium, the restoring force is Hookean, and so pico-Newton scale forces may be measured by monitoring the motion of trapped particles. The development of techniques such as holographic optical tweezers [2] and the generalized phase contrast method [3] allow real time three dimensional control of multiple optical traps, enabling the manipulation of arbitrarily shaped objects. These have some benefits over spheres when used as force probes: for example, the traps may be removed from the probe tip - the region in contact with the sample, reducing laser illumination of delicate samples, and minimising erroneous signals caused by beam occlusion due to the sample. Additional sensory information may also be extracted, such as the torque experienced by the particle and the location of the average centre of rotation [4]. A variety of non-spherical structures have been investigated, such as carbon nanotube bundles [5], micro-rods [6, 7], composite structures [8], and structures fabricated using two photon polymerisation [9].

Elongated probes exhibit varying trapping stiffnesses in different degrees of freedom, allowing us to define a preferred measurement direction - the direction in which the probe is designed to be displaced when interacting with a sample. Asymmetry can be exploited to simultaneously achieve high sensitivity in the measurement direction while maintaining position resolution in other degrees of freedom. Independent mode clamping of such a probe offers a way to further exploit this property - increasing position resolution by actively suppressing undesired motion. Position clamping is achieved by measuring the particle's displacement, and moving the traps in response to exert a force pulling the probe back towards its equilibrium position. Attention has primarily been confined to the clamping of spherical particles in two dimensions [10, 11, 12]. Recently, position clamping has been demonstrated using holographic optical tweezers, which although operating at a lower bandwidth, offer the advantages of operating in three dimensions and clamping multiple objects simultaneously [13].

In this paper we investigate the level of control we can exert over a non-spherical probe particle trapped using holographic optical tweezers. We demonstrate two dimensional translational and rotational position clamping of our probe. By independently clamping different modes, we show improved position resolution while maintaining high force sensitivity. We also demonstrate control over the average centre of rotation of our probe by varying the relative intensity of the trapping beams, and by introducing coupling terms into the clamping feedback control loop.

2. Methods

Experimental Configuration: Our holographic optical tweezers system is similar to that described in [14]. A 4 W 800 nm wavelength titanium sapphire infrared laser beam (Coherent 899) is expanded to fill an electrically addressed spatial light modulator (Boulder Nonlinear Systems, P512-0785) controlled using a LabVIEW interface, with each hologram calculation performed on the graphics card (nVidia, Quadro FX 5600) in under 1 ms [13]. The beam is then passed through a polarising beam splitter and imaged onto the back aperture of an objective lens (Zeiss Plan-Neofluor, 100 \times , 1.3 NA) which simultaneously focuses it creating the optical traps, and collects the focussed illumination light (50 W halogen bulb) from the sample. Approximately 40% of the laser beam's power is passed by the objective, and is shared

between the traps. The beamsplitter also directs light from the sample to a high-speed CMOS camera (Prosilica, EC1280). Movement of the field of view around the sample is achieved with a motorized x - y - z stage (ASI MS2000).

Probe Preparation: Our non-spherical probe particle is a cigar shaped species of diatom algae (*Nitzschia Acicularis* (Kützting) W. Smith). As these structures are naturally occurring, dimensions vary, but a typical example is $\sim 30 \mu\text{m}$ long and $\sim 5 \mu\text{m}$ wide at the centre, tapering to a tip radius of $\sim 250 \text{nm}$. This particle was chosen as it has several features that facilitate its use as a probe [15]. It has a silica shell and two frustules of higher refractive index than the surrounding structure, which act as preferential trapping points. The diatoms are trapped horizontally, parallel to the focal plane using two optical traps, one positioned over each frustule, as shown in Figure 1. The diatom is stably trapped, with all six degrees

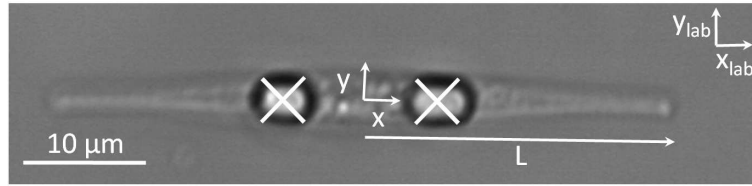


Fig. 1. Optical image of a diatom probe trapped using two optical traps (denoted by white crosses), one positioned over each frustule. x is the measurement direction. L is the distance from $x(0)$ to the probe tip.

of freedom (three translational and three rotational) constrained but undergoing Brownian motion. Using a standard illumination system we can measure three degrees of freedom - two translational (x and y) and one rotational (θ) within the focal plane, as indicated in Figure 1.

Particle Tracking: To calculate the coordinates of our probe, we employ a LabVIEW intensity thresholding algorithm similar to that described in [7], operating on each frame in real time. To obtain the probe coordinates, we track the position of the two trapping frustules which exhibit a higher intensity than the rest of the image. The centre of mass of each frustule is calculated in the “laboratory frame” (x_{lab} and y_{lab} parallel to the edges of the camera image), and averaged to find the probe position. The probe orientation θ is given by the angle between the x_{lab} axis and the line joining the centre of mass of each frustule. The equilibrium position and orientation of the probe (\bar{x}_{lab} , \bar{y}_{lab} , $\bar{\theta}$) is found by averaging 1500 laboratory frame coordinates. Once the equilibrium position has been calculated, new coordinates are transformed into the “Probe Equilibrium frame” by centering the origin at x_{lab} , y_{lab} , and rotating the coordinates by θ so the average position and orientation of the probe is zero, and x is parallel to the long axis of the probe:

$$\begin{pmatrix} x \\ y \end{pmatrix} = \mathbf{R}(\theta) \begin{pmatrix} (x_{1,lab} + x_{2,lab})/2 - x_{lab} \\ (y_{1,lab} + y_{2,lab})/2 - y_{lab} \end{pmatrix}, \quad \theta = \arctan\left(\frac{y_{2,lab} - y_{1,lab}}{x_{2,lab} - x_{1,lab}}\right) - \theta \quad (1)$$

where $\mathbf{R}(\theta)$ is the 2D rotation matrix.

3. Independent mode clamping

By reducing the laser power, we reduce the trapping stiffness of all modes within the stiffness matrix [4]. Hence we increase the sensitivity of our probe, but also reduce the position resolution of the tip. Position clamping offers a way to improve the position resolution while

maintaining a high force sensitivity. Clamping of a particular mode is achieved by relocating the traps by an amount proportional to the measured displacement from the equilibrium position. For rotational clamping, the traps are rotated about the mean trap position by an angle proportional to the measured angular displacement. For each trap position update, the required trap rotation is calculated prior to any translations as these transformations do not commute.

To ascertain whether motion in x , y and θ is correlated, we calculate the correlation matrix \mathbf{C}_r describing the correlation between different degrees of freedom within the system. To do this we normalise the covariance matrix for our measured degrees of freedom - for example the correlation between x and y (\mathbf{C}_r^{xy}) is given by $\langle xy \rangle / \sqrt{\langle x^2 \rangle \langle y^2 \rangle}$. Figure 2A shows a graphical representation of the absolute values of \mathbf{C}_r . The correlation between modes (off diagonal terms in \mathbf{C}_r) is small ($\mathbf{C}_r^{xy} = 0.081$, $\mathbf{C}_r^{x\theta} = 0.049$ and $\mathbf{C}_r^{y\theta} = 0.061$), enabling independent mode clamping. The quality of position clamping is dependent upon the reaction time between po-

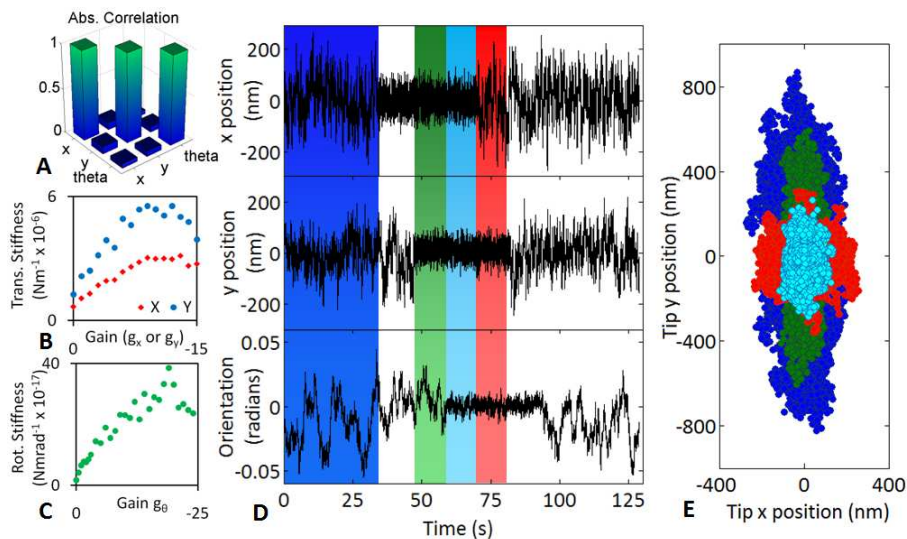


Fig. 2. (A) presents the mode correlation matrix showing minimal coupling between modes, (B) and (C) shows effective stiffnesses versus feedback gain. The lower trapping stiffness of the x -component is due to the elongation of the trapping frustules along that axis, see Figure 1. (D) shows traces demonstrating independent mode clamping. There is some limited crosstalk between different modes as the correlations are small but non zero. (E) shows the spread of probe tip positions under different combinations of clamped modes shown in (D). Dark blue indicates unclamped data. Green indicates translational clamping only. Light blue indicates all three modes simultaneously clamped, achieving the lowest tip variance. Red indicates clamping only in y and θ , therefore retaining probing functionality along the measurement direction x .

sition measurement and trap update, and the refresh rate of the spatial light modulator. In our system the maximum refresh rate of the spatial light modulator is 203 Hz, and the maximum camera frame rate over the required region of interest is ~ 600 Hz with an integration time of 1.5 ms. The reaction time from measurement of probe position to trap movement is ~ 10 ms, more details are discussed in [13]. To find the optimum gain for each mode, we measure the effective stiffness using the Equipartition Theorem at increasing gain magnitudes until instability begins to set in, as shown in Figure 2B and 2C. At the optimum gains, motion in x and y exhibits an increase in the effective stiffness by a factor of ~ 4.5 relative to the unclamped stiffness. The effective rotational stiffness exhibits an increase by a factor of ~ 22 . Figure 2D

shows independent switching of the clamping of different modes. By using optical images to approximate the length of the probe, we can use the coordinates x , y and θ to extrapolate the tip position at each measurement, as shown in the scatter graph in Figure 2E under different combinations of mode clamping.

We define a quantity f_m , the *measurement finesse*, describing the ratio between variance in the measurement direction and variance of motion orthogonal to this at the probe tip, capturing the trade-off between sensitivity and position resolution.

$$f_m = \langle x^2 \rangle / \langle y^2(\lambda) \rangle, \quad \text{where} \quad \langle y^2(\lambda) \rangle = \langle y(0)^2 \rangle + 2\lambda \langle y(0)\theta \rangle + \lambda^2 \langle \theta^2 \rangle \quad (2)$$

For small θ , $\langle y^2(\lambda) \rangle$ is the y component of variance at a point a distance λ from the equilibrium trapping position $x(0)$. To calculate f_m at the tip, we set $\lambda = L$, the tip distance from $x(0)$. The unclamped probe has a spring constant of 7.4×10^{-7} N/m in the measurement direction x . However, as it is weakly trapped to attain this sensitivity, the tip motion in the y direction has a standard deviation of 230 nm, and therefore $f_m = 0.1$. By employing position clamping in the y and θ modes, we leave the sensitivity unchanged, while reducing the standard deviation of undesired tip motion to 62 nm, improving f_m to 1.8. It is also worth noting that by sensing forces perpendicular to the long axis of the probe at the tip, the sensitivity is 8.9×10^{-8} N/m, and f_m of the unclamped motion becomes the inverse of Equation 2, $f_{m\perp} = 10$. By position clamping only the x -component of the probe motion (thin white bar in Figure 2D, scatter not shown), $f_{m\perp} = 32$ in this configuration.

4. Coupled mode clamping and control of the average centre of rotation

The point of minimum variance on the probe (which may also be considered as the probe's average centre of rotation) may be determined by minimising $\langle y^2(\lambda) \rangle$ with respect to λ :

$$\frac{\partial}{\partial \lambda} \langle y^2(\lambda) \rangle = 0, \quad \therefore \lambda_{min} = -\frac{\langle y(0)\theta \rangle}{\langle \theta^2 \rangle} \quad (3)$$

When no external forces are acting on the probe, λ_{min} coincides with the optical stress centre [4], the point at which the trapping stiffnesses of the frustules balance. By changing the relative powers in the traps, we can move the optical stress centre, and measure its displacement using Equation 3, as shown in Figure 3A. The relative trap intensity, I_{rel} , is measured using the variance of a microsphere trapped at each power and trap location. $I_{rel} = 0.5(V_{rel,x} + V_{rel,y})$, where $V_{rel,x} = (\langle x_a^2 \rangle - \langle x_b^2 \rangle) / (\langle x_a^2 \rangle + \langle x_b^2 \rangle)$, and $\langle x_a^2 \rangle$ is the x -component of the microsphere variance in trap a . $V_{rel,y}$ is similarly defined.

By varying relative trap intensity, the centre of rotation is always limited to a point between the two trapping beams. However, by introducing a non-zero coupling term into the gain matrix we may shift the centre of rotation to a point outside of the trap locations. Figure 3B shows the shift in the centre of rotation achieved using Equation 4, where α is varied between $\pm 12 \times 10^{-5}$ m/rad, coupling y and θ motion.

$$\begin{pmatrix} \Delta T_x \\ \Delta T_y \\ \Delta T_\theta \end{pmatrix} = \begin{pmatrix} g_x & 0 & 0 \\ 0 & g_y & \alpha \\ 0 & 0 & g_\theta \end{pmatrix} \begin{pmatrix} x \\ y \\ \theta \end{pmatrix} \quad (4)$$

where ΔT_i is the trap displacement of mode i , and g_i is the gain of mode i in the gain matrix. Off axis terms in the gain matrix can induce a variety of mode couplings, and could potentially be used to damp existing couplings within the motion of a complex shaped probe. Monitoring the average centre of rotation of a non-spherical probe could also be used as a delicate sensor describing a change in relative beam intensity or focussing during an experiment, for example due to beam occlusion by a sample.

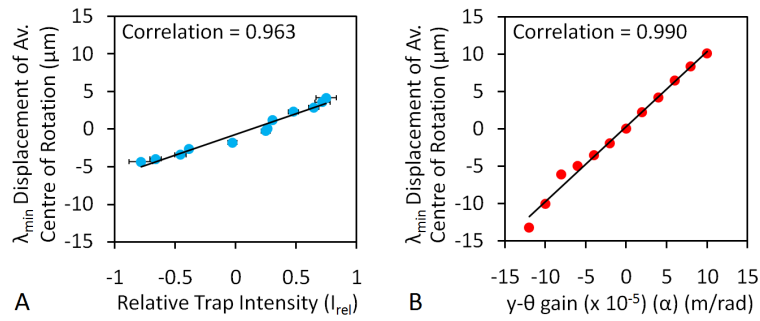


Fig. 3. Control of the location of the average centre of rotation along the length of the probe, with the traps placed $12 \mu\text{m}$ apart. (a) Control by varying the relative intensity of the trapping beams. (b) Control by variation of the y - θ term in the gain matrix enabling the centre of rotation to be moved outside the region between the two traps.

5. Conclusions

We demonstrate high-speed video-rate tracking and control of a non-spherical probe particle. Reducing the trapping laser power enables us to increase the sensitivity of our probe, at the expense of positional control of the tip. This trade-off is captured by calculation of the measurement finesse - the ratio of the variance of motion in the measurement direction to the variance of undesired motion in other measurable modes. By position clamping the y - and θ -components of the tip motion, we reduce undesired motion of the tip from a standard deviation of 230 nm to 62 nm , while retaining a sensitivity of $7.4 \times 10^{-7} \text{ N/m}$ in the measurement direction. This increases the measurement finesse by a factor of 18.

We also measure the average centre of rotation of our probe. This point may be moved along the probe length within the two trapping beams by varying the relative power in the traps. By introducing a non-zero coupling term into the position clamping gain matrix, we show that the average centre of rotation may be moved to a region outside of the two trapping beams. We use this to demonstrate control of the coupled motion of our probe, a feature that could potentially also be used to damp existing couplings within the motion of complex structures.

Using holographic optical tweezers to position clamp a non-spherical probe is an attractive option as the probe may be manipulated and position clamped simultaneously. It is also possible to extend this technique into three dimensions to fully minimise the tip motion, for example by the implementation of a stereoscopic illumination system [16]. As the efficacy of the position clamping is dependent upon the reaction time from probe position measurement to trap relocation, we expect advances in computation power and display technology may render significant improvements in the quality of position clamping with holographic optical tweezers possible in the near future.

Acknowledgments

This work is funded through an Engineering and Physical Science Research Council Grant (United Kingdom). This work was carried out with the support of the Bristol Centre for Nanoscience and Quantum Information. MJM and MJP acknowledge a Royal Society Wolfson Merit Award. We would also like to thank S. Olof, H. Rosenkranz, D. Fagan and M. Yallop for culturing the biological samples.